A new snow module improves predictions of isotope-enabled MAIDENiso forest growth model

Ignacio Hermoso de Mendoza[1], Etienne Boucher[1], Fabio Gennaretti[2], Aliénor Lavergne[3], Laia Andreu-Hayles[4,5,6], and Robert Field[7]

[1]Centre de Recherche sur la dynamique du système Terre (GEOTOP) and Centre d'études nordiques, Université du Québec à Montréal (UQAM), Canada
[2]Institut de Recherche sur les Forêts (IRF), Université du Québec en Abitibi-Témiscamingue (UQAT), Canada
[3]Carbon Cycle Research Group, Space and Atmospheric Science, Physics Department, Imperial College London, United Kingdom
[4]Tree-Ring Laboratory, Lamont-Doherty Earth Observatory of Columbia University, United States
[5]Ecological and Forestry Applications Research Centre (CREAF), Spain
[6]Catalan Institution for Research and Advanced Studies (ICREA), Spain
[7]NASA Goddard Institute for Space Studies, Dept. Applied Physics and Applied Mathematics, Columbia University, United States

Correspondence: Ignacio Hermoso de Mendoza (ihmn.zgz@gmail.com)

Abstract. The representation of snow processes in forest growth models is necessary to accurately predict the hydrological cycle in boreal ecosystems and the isotopic signature of soil water extracted by trees, photosynthates and tree-ring cellulose. Yet, most process-based models do not include a snow module, consequently their simulations may be biased in cold environments. Here, we modified the MAIDENiso model to incorporate a new snow module that simulates snow accumulation,

5   melting and sublimation, as well as thermal exchanges driving freezing and thawing of the snow and the soil. We tested these implementations in two sites in East and West Canada for black spruce (*Picea mariana*) and white spruce (*Picea glauca*) forests, respectively. The new snow module improves the skills of the model to predict components of the hydrological cycle. The model is now able to reproduce the spring discharge peak and to simulate stable oxygen isotopes in tree-ring cellulose more realistically than in the original, snow-free version of the model. The new implementation also results in simulations with

10   a higher contribution from the source water on the oxygen isotopic composition of the simulated cellulose, leading to more accurate estimates. Future work may include the development of inverse modelling with the new version of MAIDENiso to produce robust reconstructions of the hydrological cycle and isotope processes in cold environments.

1 Introduction

In boreal regions of Canada and Alaska, snow represents about 30-50% of total precipitation (Mesinger et al., 2006). This

15   feature has notable influence on hydrological and ecological system functioning in these cold environments (Beria et al., 2018). From a hydrological perspective, snowpack dynamics greatly influence water infiltration in soils, groundwater and aquifer replenishment, runoff production and water supplies to both natural and artificial water bodies during spring flood (Li et al., 2017; Barnhart et al., 2016; Berghuijs et al., 2014). From an ecological perspective, snowpack accumulation protects exposed

plant tissues and organs against cold winds (Boivin and Bégin, 1997). Snow melt contributes to mitigating the negative impacts

20 of droughts on tree growth (St. George et al., 2009), while affecting photosynthesis (Perkins and Swetnam, 1996; Peterson and Peterson, 1994). Snowpack dynamics also have the potential to alter heat fluxes, temperature and depth of freezing in soils, all of which can impact the timing of critical ecophysiological processes, driving growth in high latitude forest stands.

For decades, tree ring proxies such as ring widths (Nicault et al., 2015; Ols et al., 2018), wood density (Boucher et al., 2017) or stable isotope ratios of tree ring-cellulose (Naulier et al., 2015b, 2014; Porter et al., 2014) have been used to track inter-annual

25 changes in forest response to climate variability. Most studies emphasized on the dominant role of summer temperatures on key ecophysiological processes controlling proxy formation. This has helped to clarify the response mechanisms of the boreal forest to growing season temperatures (Gennaretti et al., 2017a) and enabled long, millennial summer temperature reconstructions to be produced in those regions (Gennaretti et al., 2017a; Naulier et al., 2015a; Gennaretti et al., 2017b). However, despite their ecological and hydrological significance, snow-related processes were rarely taken into account in these tree-ring studies

30 (Coulthard et al., 2021; Woodhouse, 2003). Consequently, the impact of these changes in snow cover properties (Meredith et al., 2019) on vegetation growth and ecolophysiological response remain highly uncertain.

Predicting the effect of snow dynamics on tree growth is a complex task as both phenomena occur in distinct seasons (Coulthard et al., 2021). Inter-seasonal heat and moisture fluxes attributable to snow need to be accounted for in order to accurately model the impact of snow on tree ring formation. The timing and magnitude of those transfers, however, result

35 from an complex interplay between snowpack properties (snow depth, density, water content) and processes that control snow accumulation and melt (precipitation, sublimation, redistribution by wind, rain on snow events, etc) (Rutter et al., 2009). Those transfers also modify the isotopic signature of the water used by trees. Indeed, snow is more depleted in the lighter isotope ^{18}O than rainfall (Kurita et al., 2004), but sublimation-driven enrichment of snow may also change the isotopic composition of the source water. Ultimately, this should be recorded in δ^{18}O of tree-ring cellulose (Beria et al., 2018). This level of complexity

40 often cannot be accounted for in correlation-based tree ring analysis, and there is a need to explicitly integrate snow dynamics in forest growth models.

Process-based models developed for tree growth are important tools to study the relationship between climate and tree-ring proxies (Guiot et al., 2014). These models are driven by meteorology and environmental variables, and integrate a wide number of equations that represent state of the art knowledge on how physical and ecophysiological processes determine tree

45 response to climate variability. A number of process-based models have been developed over the years, such as the Vaganov-Shashkin (VS) model (Fritts et al., 1991), MAIDEN (Misson, 2004), StandLeap (Girardin et al., 2008), CAMBIUM (Drew et al., 2010), ECOPHYS (Hölttä et al., 2010), Biome3 (Rathgeber et al., 2003) or the P-model (Li et al., 2014). However, despite the importance of snow for tree growth, most process-based models do not include a snow module, mostly because they were not designed to be used in boreal and alpine environments or even in mid-latitude temperate forests where snow

50 accumulates during winter. Among the previously mentioned models, the only exception is the Biome3 model (Rathgeber et al., 2003), which incorporates a basic model of snow accumulation and melt driven by air temperature, but it does not consider processes such as sublimation, energy balance or stable isotope fractionation of water isotopes during the cold season. Among the available models, MAIDEN (Misson, 2004) was specifically designed to improve the interpretation of tree-ring

proxies based on our ecophysiological knowledge about the relationship between climate and tree growth. MAIDEN simulates
the water and carbon fluxes exchanged between forests and the atmosphere, including the influence of phenology on the
production and allocation of carbon to different parts of the tree. It requires a very limited number of meteorological inputs,
which makes the application of the model possible in regions where data is scarce. The isotope-enabled version MAIDENiso
(Danis et al., 2012) incorporates calculations of the stable isotopic composition of oxygen (δ^{18}O) and carbon (δ^{13}C) in the
different components of the tree. MAIDEN was originally created for tree species in Mediterranean climates, and has been
optimized for *Quercus petraea* (Matt.) Liebl. and 12 Mediterranean species (Misson, 2004; Gaucherel et al., 2008; Boucher
et al., 2014; Gea-Izquierdo et al., 2015). Since then, the phenology and physiological processes have been adapted to simulate
tree radial growth in boreal north-eastern American forests (Gennaretti et al., 2017a) and used to simulate tree-ring cellulose
δ^{18}O in boreal and temperate forests of eastern Canada and southern South America (Lavergne et al., 2017). MAIDENiso
provides two main advantages over other process-based models: 1) It is directly comparable with tree-ring proxies. 2) It is
isotope-enabled, which allows to track water sources to the tree. However, the hydrological cycle in MAIDENiso was never
adapted to boreal conditions, and still lacks an adequate representation of snow dynamics.

Here, we incorporate a new snow module in MAIDENiso and test it against real observations. This module is driven by a
new thermal conduction model to improve the simulations when the model is used in cold environments where snow is present.
This snow module allows MAIDENiso to reproduce the basic dynamics of the snowpack, targeting a more realistic water
balance and water isotope frationation sequence, representing the δ^{18}O signal of snowfall, the sublimative fractionation at the
surface and its final imprint in tree-ring cellulose (TRC). At the same time, the snow model is simple enough to work with the
same limited number of environmental variables that MAIDENiso currently requires. We evaluate the impact of the new snow
module on the simulation of soil moisture, water outflux and the δ^{18}O signal in soil and TRC in two forest sites in Canada: a
black spruce (*Picea mariana*) forest in the Caniapiscau basin (Québec) and a white spruce (*Picea glauca*) forest in Tungsten
(Northwest Territories).

2 Materials and methods

2.1 MAIDENiso model

2.1.1 Original model

MAIDENiso (Misson, 2004; Danis et al., 2012; Gea-Izquierdo et al., 2015; Gennaretti et al., 2017a) simulates the mechani-
cal and physiological processes of a tree and its immediate environment. The model requires daily meteorological inputs of
maximum and minimum temperature, precipitation, and atmospheric CO_2 concentration (optional inputs are relative humidity,
radiation, wind speed and atmospheric δ^{13}C). MAIDENiso simulates gross primary production (GPP) and carbon allocation
on a daily basis based on inputs of meteorological and tree phenological data. Carbon is allocated explicitly to several pools
(leaves, roots, stem and a carbon reservoir) using mechanistic rules dependent on the phenology. A diagram of the model is
shown in Fig. 1, the original part of the model marked in black.

MAIDENiso simulates the hydrological processes in the immediate environment around the tree: at canopy level (interception and canopy evaporation), ground level (infiltration, evaporation and runoff) and underground (hydraulic transfers and root absorption). These processes are modelled through a series of water pools and fluxes (Fig. 2). For instance, the canopy can intercept a portion of the precipitation water up to a maximum determined by the leaf area index (LAI), which can be evaporated or dripped to the ground overnight. The surface of the soil cannot hold any stagnant water, so daily incoming water from throughfall infiltrates the soil (up to a maximum determined by soil properties) or exits the system as runoff. The soil consists of four layers of distinct thickness, with porosity and hydraulic conductivity determined by the composition of the soil, and water moves between these layers following Darcy's law. Soil water is replenished through infiltration, and depleted by root absorption for transpiration (at all layers), soil evaporation (at the upper layer) and drainage (at the bottom layer).

MAIDENiso keeps track of the stable isotopic composition of oxygen (δ^{18}O) in all the water/ice pools and fluxes of the hydrological model (Fig. 2). The isotopic module calculates fractionation from evaporation (from soil and canopy water) and transpiration at leaf level to produce an isotopic oxygen signature in TRC (δ^{18}O$_{\text{TRC}}$). This is based on the Danis et al. (2012) formulation of the Craig-Gordon model (Craig and Gordon, 1965):

$$\delta^{18}\text{O}_{\text{TRC}} = (1 - f_0) \cdot \delta^{18}\text{O}_{\text{leaf}} + f_0 \cdot \delta^{18}\text{O}_{\text{XW}} + \epsilon_0 \tag{1}$$

With δ^{18}O at leaf level being:

$$\delta^{18}\text{O}_{\text{leaf}} = \epsilon^* + \epsilon_k \cdot (1 - h_{air}) + h_{air} \cdot \delta^{18}\text{O}_{\text{V}} + (1 - h_{air}) \cdot \delta^{18}\text{O}_{\text{XW}} \tag{2}$$

Here, f_0 (unitless) is the dampening factor reflecting the exchange of the oxygen atoms between sucrose and xylem water during the synthesis of cellulose in the xylem cells of the tree rings, typically within a range of 0.4-0.5 (Roden and Ehleringer, 2000; Saurer et al., 1997; Sternberg et al., 1986; Yakir, 1992). ϵ_0 is the biochemical fractionation due to oxygen exchange between water and the carbonyl groups (C=O) in the organic molecules, undetermined but expected in a range of 24-30 ‰ (DeNiro and Epstein, 1979; Farquhar et al., 1998). ϵ^* is the equilibrium fractionation due to the change of phase of water from liquid to vapor at leaf temperature (fixed at 21.4 °C, the temperature threshold for maximum carbon assimilation), with a value of 9.65 ‰ (Helliker and Richter, 2008). ϵ_k is the kinetic fractionation due to the diffusion of vapor into unsaturated air through the stomata and the leaf boundary layer, set to 26.5 ‰ in Farquhar et al. (1989) but we consider it undetermined because it can vary over larger ranges (Buhay et al., 1996). h_{air} is the relative humidity, which is estimated in MAIDENiso from the daily air temperature and the dew point temperature (Running et al., 1987). δ^{18}O$_{\text{V}}$ and δ^{18}O$_{\text{XW}}$ are the δ^{18}O of vapor and xylem (source) water, respectively. δ^{18}O$_{\text{V}}$ is calculated from the δ^{18}O of precipitation (δ^{18}O$_{\text{P}}$) and the fractionation due to the phase change from liquid water to vapor at mean air temperature, $\epsilon^*_{T_{air}}$ (Horita and Wesolowski, 1994):

$$\delta^{18}\text{O}_{\text{V}} = \delta^{18}\text{O}_{\text{P}} - \epsilon^*_{T_{air}} \tag{3}$$

The δ^{18}O$_{\text{TRC}}$ time series produced through Eq. (1) are daily, while the δ^{18}O$_{\text{TRC}}$ measured from tree rings is commonly annually resolved, or occasionally with intra-annual resolution (e.g. Szejner et al. (2018)). To produce a yearly record comparable with observations, the daily series are weighted with GPP. This assumes that allocation of carbon to the trunk is proportional

to daily GPP (GPP_d):

$$\delta^{18}\text{O}_\text{TRC,y} = \frac{\sum_d \delta^{18}\text{O}_\text{TRC,d} \cdot \text{GPP}_\text{d}}{\sum_d \text{GPP}_\text{d}} \tag{4}$$

120   The original version of MAIDENiso (Gennaretti et al., 2017a; Danis et al., 2012) includes one snow layer, where snow accumulates and melts following changes in atmospheric temperature. This module was implemented to simulate snow reflectivity and thus changes in albedo within the calculation of the energy budget. However, this is a side-calculation that did not interact with any of the other subsystems in MAIDENiso, and thus the accumulated and melted snow was not taken into account in the water balance calculation. All water pools and fluxes in the model were liquid, regardless of temperature. In boreal climate, this

125   previous version of MAIDENiso was thus unable to predict snow accumulation during winter, and therefore did not include different source water signatures due to snowfall instead of rainfall, the fractionation of $\delta^{18}\text{O}$ due to snow sublimation, or the rapid melting of snow in spring. Therefore, this version of the model simulated unrealistic soil moisture and hydrological outflux (drainage and runoff), and too depleted values of $\delta^{18}\text{O}$ in source water in spring.

2.1.2 New implementations in the model

130   The hydrology in the new version of MAIDENiso incorporates several pools of solid water: a canopy snow pool, a single snow layer on top of the soil and a pool of ice in each soil layer (Fig. 1). In addition, the snow layer is able to hold liquid water in its porous space, adding a new pool of liquid water. These water pools and the new water fluxes are shown in Fig. 2.

Input precipitation to the system is first partitioned into rainfall and snowfall driven by the average daily temperature, following a linear partition between -2 °C and 4 °C (McCabe and Wolock, 2009). Following the same interception rule as

135   liquid water, snow can be intercepted by the canopy and added to a canopy snow pool with a maximum capacity determined by LAI, from where it can sublimate. However, while the canopy water pool is always emptied at the end of each day, the canopy snow pool does not. Canopy snow can still drip to the ground based on atmospheric temperature, following a drip model taken from the Community Land Model version 5 (CLM5) (Lawrence et al., 2019).

A single, uniform snow layer can cover the uppermost soil layer fully or partially, keeping track of snow thickness and the

140   masses of snow and liquid water in the layer, calculating the density of the layer dynamically. Freezing transfers water to snow mass without changing thickness, thus increasing density (with pure ice density as maximum), while melting and sublimation remove snow mass but keep density constant. The snow layer is forced to have a minimum thickness of 0.1 m (which is needed for numerical convergence), so the partial snow cover is decreased to avoid a thickness below this minimum (i.e. partial cover of zero when no snow is present). While snowfall always accumulates over the existing snow layer, increasing mass and thickness

145   according to a temperature-variable density model of newly fallen snow (van Kampenhout et al., 2017), the portion of rainfall that hits the snow layer is determined by the partial snow cover. Sublimation from the snow layer is calculated by modifying the version of the Penman-Monteith equation (Stigter et al., 2018):

$$\lambda E_{pot,snow} = \frac{\Delta \cdot R + \rho_{air} \cdot C_P \cdot \delta_{atm}/r_a}{\Delta + \gamma} \tag{5}$$

Δ (kPa $°C^{-1}$) is the gradient of the saturation vapor pressure curve, γ (kPa $°C^{-1}$) is the psychrometric constant (Loescher

150   et al., 2009), R (MJ) is the net radiation over the snow surface, ρ_{air} (kg m^{-1}) is the air density, C_P (MJ kg^{-1}) is the specific

heat of dry air, and r_a (s m^{-1}) is the aerodynamic resistance to water vapor transfer. r_a typically depends on several factors,

e.g. wind (Blanken and Black, 2004). However, wind data is not available in tree-ring sites, which makes formulas dependent

on the wind unusable. Here, we assume a constant r_a but optimize its value for each site using the available data of snowfall

and snow pile's thickness and mass.

155   A pool of ice has been added to each soil layer. The pools of liquid water and solid water (ice) in each layer compete for the

same porous space, so the ice content of a soil layer decreases its effective porosity. This decreases both the maximum amount

of liquid water the layer can hold, and the hydraulic conductivity of the layer. Soil ice increases when soil temperature is below

$0\,°C$, and decreases when soil temperature is above $0\,°C$.

To calculate the change in water phase from solid to liquid in the snow and soil layers, we have added a one dimensional

160   (vertical) thermal conduction model largely based on CLM5 (Lawrence et al., 2019). In this model, the system formed by the

snow-soil layers is bounded at the top (as soil or snow) by the heat flux from the overlying atmosphere, and at the bottom by

a constant value representing the geothermal heat flux. The amount of water (or ice) that freezes (or melts) is calculated from

the deficit (or excess) of energy to keep the temperature of the layer at $0\,°C$.

The new implementation of snow in MAIDENiso is now able to reproduce the dynamics of the snowpack, which influences

165   the rest of the components of the model (Fig. 1). The accumulation of the winter precipitation increases the amount of water

available in the soil in spring, which in turn favors the onset of photosynthesis. A higher photosynthetic activity results in more

carbon assimilated by the canopy, potentially leading to a shorter budburst phase. A diagram showing the links between the

different components in MAIDENiso is shown in Fig. 1.

The new MAIDENiso version also includes new isotopic fractionation processes for the sublimative fluxes, and for the phase

170   changes between liquid water and ice. In cold regions where snowfall is a considerable portion of the yearly precipitation,

fractionation from snow sublimation is expected to produce a significant enrichment of the $\delta^{18}O$ isotopes in the snow layer,

which after melting is incorporated in the soil water, and ultimately in TRC.

2.2   Calibration of MAIDENiso

Different parameters that are species-dependent and site-dependent need to be defined before running MAIDENiso at a partic-

175   ular site. Most of these parameters can be obtained from direct observations at the studied site, such as the characteristics of

the soil (composition and depth), or the root-leaf proportions of the tree species. However, when the values of the parameters

are unknown, these are calibrated through a Bayesian optimization algorithm described in detail in Gennaretti et al. (2017a).

This optimization is based on Markov chain Monte Carlo (MCMC) sampling that retains combinations (blocks) of parameters

that satisfy a condition, maximizing the coincidence between a series of observations and the equivalent products simulated

180   by MAIDENiso. Here,we used 50 independent chains of parameter blocks and selected the most optimal block of parameters

(called the "plausible block").

The series of observations used in the MCMC consist of observed time series of snow (depth or mass of the snowpile), GPP and $\delta^{18}O_{TRC}$. The parameters to be determined via MCMC for each subsystem of the model are the following:

- Snowpile: 1 parameter, r_a from Eq. (5). Calibrated by comparing observed and simulated daily Snow Depth (SNDP).

185
- GPP: 6 parameters (see appendix A). Calibrated by comparing observed and simulated daily GPP.

- $\delta^{18}O_{TRC}$: 3 parameters, f_0, ϵ_0 and ϵ_k in Eqs. (1) and (2). Calibrated by comparing observed and simulated yearly $\delta^{18}O_{TRC}$.

Because the new and the original versions of MAIDENiso behave differently, an independent calibration of the parameters is needed to run each of them. Note that the original version of MAIDENiso does not need to be calibrated for the snow
190 parameters because it does not include a snow module.

Some parameters can influence more than one process indirectly, e.g. the snowpile affects source water and therefore $\delta^{18}O_{TRC}$, or the GPP parameters control the amount of carbon produced, which in turn affects $\delta^{18}O_{TRC}$. To avoid that the calibration of some processes affects parameters that are already calibrated, the parameter sets need to be calibrated in a specific order: Snow first, GPP second, and lastly $\delta^{18}O_{TRC}$.

195 ## 2.3 Study sites and input meteorological data

The studied tree-ring sites are located in Tungsten, Northwest Territories, Yukon border (61.98° N, 128.25° W, 1145 m a.s.l.) and in the Caniapiscau basin, Quebec (54.86° N, 69.72° W, 530 m a.s.l.).

MAIDENiso requires daily meteorological inputs for a continuous period of time overlapping with the period of available observations. Daily CO_2 data were obtained from the Mauna Loa Observatory observations (Keeling et al., 1976) corrected
200 with the CarbonTracker measurement and modeling system (Peters et al., 2007).

The closest meteorological stations to the studied sites were located 100 km away from Tungsten and 186 km from Caniapiscau. Therefore, temperature and precipitation data were taken from the NARR (North American Reanalysis) dataset (Mesinger et al., 2006) at the coordinates of the studied sites. The NARR has a spatial resolution of 32.5 km × 32.5 km and spans for the period 1979-2013. Meteorological inputs were also needed at two additional sites to calibrate GPP, which will be described in
205 detail in section 2.4.

MAIDENiso also needs information about $\delta^{18}O_P$. Two different approaches can be used to infer $\delta^{18}O_P$: The first and most direct way is to use daily values of $\delta^{18}O_P$ as another meteorological input. However, these values are not always available. The second approach, which we used here, is to estimate three parameters (a, b and c) from a linear regression model based on precipitation (P, mm), air temperature (T_{air}, °C) to obtain the $\delta^{18}O_P$ values:

210 $$\delta^{18}O_P = a \cdot T_{air} + b \cdot P + c \tag{6}$$

This approach has the advantage that, once the model has been obtained, the parameters can be used with datasets other than the dataset used for its calibration. In this paper, we calibrated this regression model using meteorological data from

the gridded dataset IsoGSM (Yoshimura et al., 2008) from the grid points that contain the coordinates of the Caniapiscau and Tungsten sites. We discarded the direct use of the IsoGSM meteorological and $\delta^{18}O_P$ data into MAIDENiso because the

215   precipitation quantities derived from IsoGSM were too low for these sites. However, the IsoGSM meteorological data was still useful to obtain the parameters for our regression model. We obtain different equations for liquid (rainfall) and solid precipitation (snowfall) using separately data corresponding to temperatures below -4 °C for snowfall and higher than 2 °C for rainfall (see Table 1).

2.4   Tree-Ring $\delta^{18}O$, GPP and snow data

220   We used published $\delta^{18}O_{TRC}$ chronologies for Tungsten (Field et al., 2021) and Caniapiscau (Nicault et al., 2014). These chronologies span between 1900-2003 for Tungsten and 1948-2013 for Caniapiscau, however we only considered the isotopic records for periods that overlap with the NARR meteorology: 1979-2003 for Tungsten and 1979-2013 for Caniapiscau.

We used GPP data available from the closest eddy covariance flux stations to estimate the parameters controlling GPP at the studied sites, assuming that the obtained parameters were similar at the studied sites. To calibrate GPP in Tungsten, we

225   used the University of Alaska Fairbanks (Uaf) station from the Ameriflux network (64.87° N, 147.85° W; data spanning the 2003-2018 period;Ueyama et al. (2021)) at 1023 km from our study site. For Caniapiscau, we obtained daily GPP data from an eddy covariance station located in a mature black spruce forest in northern Quebec ("Quebec Eastern Old Black Spruce station" - EOBS; 49.69° N, 74.34° W; http://fluxnet.ornl.gov/site/269; with data spanning the 2003-2010 period, Bergeron et al. (2007)) at 650 km from our study site. MAIDENiso was used to simulate GPP at both stations, but we needed additional

230   meteorological inputs. For the Uaf station, we used the meteorological inputs available at the station. For the EOBS site, the meteorological inputs were taken from the gridded interpolated Canadian database of daily minimum-maximum temperature and precipitation for 1950-2015 (Hutchinson et al., 2009), used in Gennaretti et al. (2017a).

In-situ snowpile data are needed to test the predictive skills of MAIDENiso to simulate the snowpile. Snow Water Equivalent (SWE) is the ideal snowpile data to use because addition (from precipitation) and removal (from sublimation and melting) of

235   snow to or from the snowpile is calculated in units of mass. Alternatively, snow depth (SNDP) data, most commonly available, can be used as well to compare with observations but requires knowledge about snow density. SWE field measurements were only available for the Caniapiscau site at discrete (biweekly) intervals during Winter and early Spring between 1971-1993 (data provided by Hydro-Québec, personal communication). Therefore, in order to make the results from both sites comparable, we used SNDP data from NARR to calibrate the snowpile at Tungsten and Caniapiscau and only used the SWE measurements at

240   Caniapiscau to validate the simulations.

2.5   Model evaluation and experiments

To evaluate the agreement between observed and simulated $\delta^{18}O_{TRC}$ for the two versions of MAIDENiso, we calculated the Pearson correlation coefficient and associated p-values (p < 0.05 were considered significant). To evaluate the coincidence between the observed and simulated water discharge, we used the Nash-Sutcliffe model Efficiency (NSE) coefficient (Nash

and Sutcliffe, 1970), which is equivalent to a coefficient of determination:

$$\text{NSE} = 1 - \frac{\sum_t (Q_m^t - Q_o^t)^2}{\sum_t (Q_o^t - \overline{Q}_o)^2} \tag{7}$$

where Q_m^t and Q_o^t are the modelled and observed discharge at time t, respectively. The NSE ranges between $-\infty$ and $+1$. To facilitate the interpretation of NSE, we rescaled the NSE within the range of (0,1) with the Normalized Nash-Sutcliffe Efficiency (NNSE) coefficient (Nossent and Bauwens, 2011):

$$\text{NNSE} = \frac{1}{2 - \text{NSE}} \tag{8}$$

To estimate the effect of the new snow module on predictions of $\delta^{18}O_{\text{TRC}}$, we compared the parameters influencing $\delta^{18}O_{\text{TRC}}$ obtained by independent calibrations.

We also investigated the relative contributions to $\delta^{18}O_{\text{TRC}}$ of the source (xylem) water and of the fractionation processes during transpiration in the leaf. Using the same approach as in Lavergne et al. (2017), we compared the predicted $\delta^{18}O_{\text{TRC}}$ from the reference simulations with those obtained from two experiments. First, to isolate the contribution of the source water on $\delta^{18}O_{\text{TRC}}$, we set the relative humidity (h_{air}) and $\delta^{18}O_V$ constant using the average values of h_{air} and $\delta^{18}O_V$ obtained from the reference simulations. Second, to isolate the contribution of the isotopic enrichment of the leaf water during transpiration on $\delta^{18}O_{\text{TRC}}$, we set $\delta^{18}O_{\text{XW}}$ constant using the average value of the reference simulation. We then compared the reference and experimental simulations using the coefficient of determination (R^2).

3 Results

3.1 Snow calibration and impact on hydrology

A comparison of the SWE simulated by MAIDENiso with an estimate of SWE based on the SNDP obtained from NARR (using the snow density simulated by MAIDENiso) at the Tungsten and Caniapiscau sites, and with the discrete SWE data at the Caniapiscau site, are shown for both sites in Fig. 3.

MAIDENiso was able to reproduce the general shape of the temporal change of the snowpile and showed a similar pattern to the real SWE observations collected at the Caniapiscau site (Fig. 3b). In contrast the NARR-based SWE estimates showed different magnitudes of the snowpack during the winter months and the offset timing of snow accumulation and melting. The discrepancies between the NARR-based SWE data and the MAIDENiso SWE simulations could arise from a mismatch between the NARR meteorology (used to drive the model) and the NARR's snowpile data, which according to the available documentation was artificially increased to match other sources (Mesinger et al., 2006). Therefore, our SWE simulations computed using the MAIDENiso were in better agreement with the direct observations of SWE at the site than were the SWE data obtained directly from the NARR dataset.

The calibration process converged and constrained the values of r_a well (resistance to water vapor transfer) at both sites, as shown in Table 2. The values obtained for both sites were quite different, equal to 47.88 s m^{-1} in Caniapiscau but to

275   87.35 s m^{-1} in Tungsten. This potentially indicates that the physical factors that are neglected when assuming a constant r_a (such as wind speed) are quite different between the two sites. The higher values at Tungsten indicates that snow sublimates at a slower rate, likely because the average wind speed during winter at this site is smaller than at Caniapiscau.

The implementation of snow and ice pools into MAIDENiso resulted in a significant improvement of the realism of the hydrological outputs of the model. Some hydrological outputs that can be simulated are for example the water outflux (liquid

280   water leaving the system), which in the model takes the form of runoff (water overflowing the infiltration capacity of the soil) and drainage (downwards water flux from the lowest soil layer). Figure 4 shows the combined runoff and drainage simulated by MAIDENiso with and without including the snow module and the scaled observations of river discharge in the Caniapiscau basin. The observations show a peak in river discharge between May and July, corresponding to the melting of the snow accumulated during winter. In the simulations computed using the original version of MAIDENiso (without snow module) the

285   outflux of the model resembled the pattern of precipitation during the year because all incoming precipitation was considered as liquid. Conversely, our new MAIDENiso version (with snow module) does not have any outflux during winter, when all water is in solid state, and reproduces more accurately the peak of water outflux during spring melting. Overall, the timing of the spring discharge was well reproduced by the MAIDENiso version with snow, while the original version was unable to produce this peak. This improvement is confirmed by the NNSE between the observed and modelled river discharge at Caniapiscau

290   which was NNSE = 0.1 for the model without snow and NNSE = 0.45 for the new model with snow.

3.2   GPP calibration

GPP was calibrated twice at each station: first for the original version of MAIDENiso and second for the new version with snow. Both versions were able to predict GPP observations, and in a similar way for both the Uaf and the EOBS stations (Fig. 5). The observed and simulated GPP were in good agreement regarding the timing (onset and offset) of the yearly peaks.

295   The maximum of these peaks was higher for the observations, but this is due to exceptional days of very high observed GPP. Overall, the average GPP during the growing season was well reproduced at both GPP stations.

3.3   Effects of the snow module on δ^{18}O

Both model versions (MAIDENiso with and without snow) reproduced the mean level of the $\delta^{18}O_{\text{TRC}}$ series (Fig. 6). This was expected because 1) the calibration process maximized the coincidence between observed and simulated $\delta^{18}O_{\text{TRC}}$, and

300   2) the biochemical and kinetic fractionation parameters ϵ_0 and ϵ_k could compensate the mean level of $\delta^{18}O_{\text{TRC}}$ in Eq. (1) for differences in $\delta^{18}O_{\text{XW}}$. Regarding the agreement between inter-annual variations, the observed and simulated $\delta^{18}O_{\text{TRC}}$ were not significantly correlated when snow was absent in the model (p > 0.20; Fig. 6), but they were significantly correlated when MAIDENiso included snow (r = 0.57 in Tungsten and r = 0.52 in Caniapiscau, p < 0.01; Fig. 6). Both versions of the model were unable to match the yearly variability of the observed $\delta^{18}O_{\text{TRC}}$ at Caniapiscau, which makes it difficult to appreciate

305   the improvement in the correlation between simulated and observed $\delta^{18}O_{\text{TRC}}$ when adding snow to the model in Fig. 6b. To facilitate the interpretation of Figs. 6a, b, we have standardized the observed and simulated $\delta^{18}O_{\text{TRC}}$ series (transformed to mean 0 and standard deviation 1) in Figs. 6c, d.

The improvement on the simulated $\delta^{18}O_{TRC}$ by the new version of MAIDENiso is difficult to appreciate in Fig. 6, specially at the site of Caniapiscau due to both versions of the model being unable to match the yearly variability of the observed
310 $\delta^{18}O_{TRC}$. To facilitate the interpretation of this figure, we have standardized the observed and simulated $\delta^{18}O_{TRC}$ series (transformed to mean 0 and standard deviation 1) in Fig. 6c,d.

The distribution of the optimized parameters controlling $\delta^{18}O_{TRC}$ can help to understand how the model compensated for the presence or absence of snow (Table 2 and Fig. 7). For instance, a lower value for the dampening factor than the expected range of $f_0 = 0.4 - 0.5$ obtained from previous studies (Roden and Ehleringer, 2000; Saurer et al., 1997) would indicate
315 that the model does not simulate the $\delta^{18}O_{XW}$ signal correctly. Higher values of the biochemical fractionation ϵ_0, or the kinetic fractionation ϵ_k, in one version of MAIDENiso than the other, would indicate that the model is compensating for comparatively lower values of $\delta^{18}O_{XW}$ and/or $\delta^{18}O_V$ in Eqs. (1,2). In our simulations, adding snow induced an increase in the dampening factor f_0 at both sites, suggesting that the signal of the source water on $\delta^{18}O_{TRC}$ was stronger than without considering snow.

To better understand the effect of the snow module on $\delta^{18}O$, we compared $\delta^{18}O$ values from various parts of the model
320 (precipitation, xylem water, leaf water and TRC), for both versions (with and without snow) of MAIDENiso at the two studied sites (Fig. 8). The snow directly impacted the $\delta^{18}O$ of the source (xylem) water, $\delta^{18}O_{XW}$ (Fig. 8b). Without the snow module, $\delta^{18}O_{XW}$ followed closely the isotopic signal of the precipitation ($\delta^{18}O_P$) shown in Fig. 8a, with a delay due to the isotopic mixing in the soil, and it was slightly enriched due to isotopic fractionation during soil and canopy evaporation. When snow was present in the model, the soil absorbed melted water from the snowpile in spring, which was enriched due to fractionation
325 during sublimation in winter. $\delta^{18}O_{XW}$ was higher than in the version without snow. The difference in $\delta^{18}O_{XW}$ values between the two versions reduced with time with the infiltration and mixing of the enriched summer precipitation.

The daily $\delta^{18}O$ in the leaf and the TRC calculated with Eqs. (1) and (2) are shown in Figs 8c and 8d. The existence of the snow layer induced a higher $\delta^{18}O$ at the leaf level, especially in spring, due to the higher $\delta^{18}O_{XW}$ level. The mean level of $\delta^{18}O_{TRC}$ did not change after adding snow, despite the enrichment of $\delta^{18}O_{leaf}$ and $\delta^{18}O_{XW}$, because it was compensated by
330 the lower values of the biochemical fractionation ϵ_0.

3.4 Relative influence of xylem water and leaf-level processes to the $\delta^{18}O_{TRC}$ signature

Finally, we investigated the relative contributions from the $\delta^{18}O$ of xylem water and the leaf transpiration enrichment of $\delta^{18}O$ on the $\delta^{18}O_{TRC}$ timeseries (Fig. 9). At both sites, the leaf water $\delta^{18}O$ isotopic enrichment had a stronger influence on $\delta^{18}O_{TRC}$ than the $\delta^{18}O$ variability of xylem source water, as shown by the higher variance explained by the experiment that simulated
335 $\delta^{18}O_{TRC}$ considering only the effect of $\delta^{18}O$ leaf water enrichment (higher R^2).

The addition of snow increased the coefficient of determination for both types of experiments, but more importantly for the xylem source water experiment. This was in agreement with the increase in f_0 seen in Table 2 for both sites, pointing to an important influence of snow on the source water and on $\delta^{18}O_{TRC}$.

4 Discussion

340 In this study, we implemented a new snow module in MAIDENiso to simulate snowpack dynamics and improve the model representation of the soil hydrology and the isotopic fractionation of oxygen in water and tree-ring cellulose. In the following paragraphs we discuss the impacts of the snow module addition on the different components of the model (i.e. the hydrological, photosynthetic and $\delta^{18}O$ modules), addressing the skills and limitations of our approach. We also discuss the implications of our new snow module implementation in MAIDENiso for future studies.

345 ### 4.1 Improvements of the hydrological module

The skills of MAIDENiso to reproduce the hydrological cycle improve with the addition of the snow module. Thanks to the accumulation of the snow and later melting, the new version of MAIDENiso is now able to simulate the observed peak of river discharge in early spring, while the previous version without the snow module could not simulate any peak (Fig. 4). The magnitude of this peak cannot be compared directly with observations, because downscaling the river discharge by the size of

350 the basin is not enough to make a direct comparison. The water outflux simulated by MAIDENiso is the surface runoff (which is incorporated immediately to the streams) plus the subterranean drainage (which takes a longer time to reach the stream). Also, the outflux from different points of the basin takes different times to reach the main stream of the basin, and the outflux over the whole area of the Caniapiscau basin is not necessarily identical. A routing model (Oki et al., 1999; Southworth et al., 2007; Miller et al., 1994) could be used to calculate the delay and flow to the main stream from across the whole basin, for

355 both types of water outflows. The incorporation of a routing model in MAIDENiso would allow to produce an estimate of streamflow for a basin, which would allow direct comparison with river discharge observations.

4.2 No effects of snow on photosynthesis

The calibration process yielded two different sets of parameters when using the two versions of the model but resulted in similar predicted GPP values. However, for both versions of MAIDENiso, we obtained very similar posterior distributions and

360 values in the plausible block for the parameters controlling GPP (Table A1, Figs A1, A2). These similarities indicate that, at our study sites, photosynthesis is not very sensitive to the availability of additional water from snow melt, suggesting radial tree growth is not limited by water availability. This was expected, because in high latitudes soil humidity is not a major constraint on tree growth and trees are usually mostly sensitive to temperature (Boisvenue and Running, 2006; D'Orangeville et al., 2018). Different results could be found in other sites where trees are more dependent on water derived from snowmelt

365 (Du et al., 2014). Because GPP is not affected by the snow module, our study sites are ideal to investigate the effects of snow on $\delta^{18}O_{TRC}$ variations because it allows us to discard GPP as a possible cause for the differences observed between the two model versions.

4.3 Effects of snow on xylem water, leaf and tree-ring cellulose δ^{18}O

Following the approach proposed by Lavergne et al. (2017), we produced yearly $\delta^{18}O_{TRC}$ timeseries by weighting the daily
370 values with the GPP, assuming that C allocation to the stem is proportional to GPP. MAIDENiso has a module for the allocation of available C to the different parts of the tree, which provides an alternative and more realistic way of calculating yearly $\delta^{18}O_{TRC}$. However, the calibration of this module ideally requires observations of the same units as the product of the allocation module, i.e. C mass per unit of stand basal area allocated to the stem. TRW observations can be used, but they represent an approximation and do not offer an intra-annual C allocation pattern to constrain the simulations. Therefore, the use of GPP
375 to weight the daily $\delta^{18}O_{TRC}$ was the best option.

The calibration of the δ^{18}O processes for the two versions of MAIDENiso and the two sites yielded significant differences in the optimized parameters, both in the distribution of the optimal blocks and the values in the plausible blocks (Fig. 7, Table 2). The dampening factor f_0, which controls the direct contribution of the source water to the $\delta^{18}O_{TRC}$ signal, was significantly higher (especially in Tungsten) after adding snow. The calibration of the original model converged to a value of $f_0 \approx 3.2$, with
380 the posterior distributions pushing toward the lower prior limit of 0.3 (Table 2, Fig. 7), which suggests that the calibration procedure would have converged towards a smaller value if it had been allowed. Adding snow increased the dampening factor to $f_0 = 0.48$ in Tungsten and $f_0 = 0.43$ in Caniapiscau, in agreement with the range of $f_0 = 0.4 - 0.5$ reported in previous studies (Roden and Ehleringer, 2000; Saurer et al., 1997; Sternberg et al., 1986; Yakir, 1992). Lavergne et al. (2017) obtained a dampening factor of $f_0 = 0.41$ in Quebec using the original model, because the parameters from Eq. (6) could be calibrated
385 to compensate for the absence of snow. These findings indicate that the addition of snow allows the model to increase the contribution of the source water to $\delta^{18}O_{TRC}$.

The calibrated value for the biochemical fractionation ϵ_0 was different at the two sites, ranging around 27.41-27.85 ‰ in Tungsten and 24.15-24.48 ‰ in Caniapiscau. The kinetic fractionation ϵ_k obtained at the two studied sites also differed strongly, from 11.8-13 ‰ at Tungsten to 22.8-23.4 ‰ at Caniapiscau (Table 2). ϵ_k was set to 26.5 ‰ by Farquhar et al. (1989),
390 but it can vary over a larger range (Buhay et al., 1996). Lavergne et al. (2017) obtained a value of $\epsilon_k = 17.20$ ‰ for Quebec, with a similar posterior distribution that the one obtained here.

Our analysis also shows that the leaf ^{18}O enrichment due to transpiration has a stronger influence on $\delta^{18}O_{TRC}$ than the isotopic composition of the source (xylem) water, both in Tungsten and Caniapiscau, suggesting that it is the main driver of $\delta^{18}O_{TRC}$ variations. These results are in agreement with Lavergne et al. (2017) findings and reflect the strong effect of vapour
395 pressure deficit on $\delta^{18}O_{leaf}$.

The addition of the snow module to MAIDENiso therefore frees the calibration process from having to overcompensate for the artificially depleted values of $\delta^{18}O_{XW}$ during the growing season (Fig. 8b). As our results have shown, this significantly increased the correlation between the observed and simulated $\delta^{18}O_{TRC}$ compared to the version without snow (Fig 6; r = 0.52 for Caniapiscau and r = 0.57 for Tungsten, p < 0.01 versus non-significant, respectively). The improvement of the predictive
400 skill of the model with the snow module reflects the influence of winter precipitation on physiological processes. Without snow,

all winter precipitation passes through and out of the hydrological system without affecting the trees. In contrast, including snow allows winter precipitation to affect $\delta^{18}O_{TRC}$ indirectly through the source water.

Overall, the improvements found in the $\delta^{18}O_{TRC}$ simulations at both sites indicate that snow plays a critical role in $\delta^{18}O$ of the source water and thus on the final signature of $\delta^{18}O_{TRC}$. Even if the addition of snow would not had resulted in a significant improvement of the correlation between the simulated and observed $\delta^{18}O_{TRC}$, accounting for snow-related processes along the mechanistic chain is necessary for the application of a process-based model in an environment where snow is present. Process-based models are useful to understand complex processes, and while they may not necessarily produce better simulations (closer to observations) than response functions, they can be used under different conditions from those of the data used for their calibration (Guiot et al., 2014). The incorporation of the snow module in MAIDENiso is therefore required for predicting tree-ring isotopic composition in forests located in cold environments where snow is present.

4.4 Implications for future studies

Based on our results and comparison with other studies, we can conclude that the snow module predicts more realistic and robust fluxes of water within the soil-plant-atmosphere continuum. The improvement of MAIDENiso to disentangle the contribution from the source (xylem) water and the $\delta^{18}O_{leaf}$ enrichment signal on $\delta^{18}O_{TRC}$ can help to track the origin of the isotopic signal and eventually improve the interpretations of the climate signal recorded in the tree rings. This is important because tree-ring isotopes are important climate proxies (Cernusak and English, 2015). The inclusion of the new snow module in the model can provide a more accurate representation of the physical and physiological processes taking place than in earlier studies which ignored the additional effects of snowpack dynamics on $\delta^{18}O_{TRC}$, e.g. Lavergne et al. (2017). Now, MAIDENiso can simulate more reliably the interaction between the coupled water and carbon cycles and the tree physiology in cold environments. The uncertainties in the predictions of the response of forest productivity to hydrological changes may also be reduced, leading to better forward predictions that can eventually be used to reconstruct seasonal and long-term hydroclimatic variations.

An inverse modelling approach has previously been developed and tested using MAIDENiso to reconstruct paleoclimate from tree-ring data in the Fontainebleau Forest, France (Boucher et al., 2014). However, this exercise was restricted to the reconstruction of meteorological variables during summer, and to regions where the tree-ring proxies were not significantly affected by winter meteorology. The inclusion of snow in the model opens new possibilities for reconstructing hydroclimate in cold regions, now that the simulation of $\delta^{18}O_{TRC}$ accounts for snow-related processes.

5 Conclusions

In this paper we presented the new snow module incorporated into MAIDENiso, which consists of new hydrological calculations of snow dynamics and a thermal module. Our findings show how this snow module improves the simulation of outputs associated with the hydrological cycle at cold and high latitudes without affecting simulations from the carbon cycle component. These findings were expected because GPP and tree-ring growth at the studied boreal high-latitude sites are not

constrained by soil moisture availability but by surface air temperature and light (Jarvis and Linder, 2000). The simulations of the new version of MAIDENiso reproduce the observed $\delta^{18}O_{TRC}$ better than the original snow-less version of MAIDENiso.

435 Based on the development presented here, the potential for the application of MAIDENiso is notably increased.

Code and data availability. The MAIDENiso code will be made available upon publication of this paper. The meteorological data and the observational data are available in the Zenodo repository (https://doi.org/10.5281/zenodo.5095718).

Appendix A: Photosynthesis model

GPP ($g\,C\,m^{-2}\,day^{-1}$) in MAIDENiso derives from a coupled photosynthesis-stomatal conductance system. The leaf photo-
440 synthesis is modelled following Farquhar et al. (1980), scaled to the canopy followingDe Pury and Farquhar (1997) as explained in Misson (2004). Daily Vcmax ($Vcmax_i$) is modelled as:

$$Vcmax_i = \frac{Vmax}{1 + \exp(Vb \cdot (Tday_i - Vip))} \tag{A1}$$

The parameter Vmax determines how daytime temperature Tday controls the maximum carboxylation rate at day i. Because there was no explicitly known mechanistic formula relating Vcmax and Tday, three parameters were introduced to control this
445 relationship in a non-linear way, i.e. Vmax, Vb and Vip. These parameters control the asymptote, the slope and the inflection point of Vcmax, respectively, and have to be calibrated.

The stomatal conductance for carbon ($\mu mol\ m^{-2}\ s^{-1}$) is calculated using the Leuning et al. (1995) model, modified by Gea-Izquierdo et al. (2015) to incorporate soil water stress:

$$g_{sc} = g_0 + g_1 \frac{A_n}{(C_a - \Gamma^*)(1 + VPD/VPD_0)} \theta_g\ P_{atm} \tag{A2}$$

450 where $g_0 = 0\mu mol\ m^{-2}\ s^{-1}$ and $g_1 = 10\mu mol\ m^{-2}\ s^{-1}$ are fitted parameters representing the residual conductance as the net assimilation rate (A_n) approaches zero and the slope of the function, respectively. P_{atm} is the atmospheric pressure (Pa). C_a is the atmospheric CO_2 pressure (Pa). Γ^* is the CO_2 compensation point in the absence of dark respiration (Pa), which is calculated following Bernacchi et al. (2001). VPD is the vapor pressure deficit (kPa), and VPD_0 is an empirically fitted parameter representing the sensitivity of stomata to changes in VPD (usually around 15 kPa; Knauer et al. (2015)). θ_g is the
455 empirical soil water stress factor, a non-linear function ranging between 0 when the soil is too dry for the roots and 1 in absence of water stress:

$$\theta g = \frac{1}{1 + \exp(soilb \cdot (SWC_i - soilip))} \tag{A3}$$

The water stress level depends on the soil water content (SWC, mm), but the current version of MAIDENiso lacks a mechanistic model to explain the relationship between soil water content and water stress. For this reason, this relation is modelled
460 as a logistic function, introducing the calibration parameters soilb and soilip as the slope and the inflexion point of θg.

Finally, there is a time lag between the recovery of photosynthesis and the temperature increase in spring that is taken into account by the model. This is done by replacing Tday in Eq. (A1) by the temperature transformation S, defined as:

$$\frac{dS_i}{di} = \frac{Tday_i - S_i}{\tau} \tag{A4}$$

where τ is a parameter representing the number of days needed by the tree to adapt the photosynthesis to changing temper-
465 atures.

There are a total of 6 undetermined parameters that control GPP production in MAIDENiso in Eqs. (A1), (A3) and (A4). These parameters were calibrated at the two eddy covariance flux stations described in section 2.4, for both versions of the model. These parameters, their prior distributions and their posterior distributions are shown in Table A1. For better visualization, the probability distribution function (pdf) of the posterior distributions of the GPP parameters are also shown in Figs. A1
470 and A2.

Author contributions. I.H.M. implemented the new snow module into MAIDENiso, performed the simulations and analyses and wrote the first draft of the manuscript. F.G. and A.L. helped in setting up the new module into the original version of the model. L.A.-H, R.F. and E.B. provided the $\delta^{18}O_{TRC}$ chronology. E.B., L.A.-H, F.G. and A.L. contributed to the design of the study (analyses to perform and structure the paper), and interpretation of the results. All authors contributed to improve the manuscript and guided the simulations and analyses.

475 *Competing interests.* The authors declare that they have no conflict of interest.

Acknowledgements. This research was supported by the Natural Sciences and Engineering Research Council of Canada (NSERC) PERSIS-TENCE project (RDC 485475 - 15 to E.B.), and the US National Science Foundation (NSF) grants PLR-1504134, PLR-1603473, AGS-1502150 and OISE-1743738 awarded to L.A-H. The PERSISTENCE project is a collaborative research grant that involves the participation of Hydro-Québec, Manitoba Hydro and the Ouranos consortium. We thank L. Perreault and D. Tapsoba from Hydro-Québec for providing the
480 SWE data at the Caniapiscau basin used here. A.L was supported by a Marie Sklodowska-Curie Individual Fellowship under the European Union's Horizon 2020 Research and Innovation Programme (grant agreement no: 838739 ECAW-ISO). F.G. was supported by the Ministère des Forêts, de la Faune et des Parcs (MFFP; contract number 142332177-D), and NSERC (Alliance Grant number ALLRP 557148-20). We are thankful to Wei Huang and Jean-Francois Hélie, respectively from the Stable Isotope Laboratory of Lamont-Doherty Earth and GEOTOP (UQAM), for their support with isotopic measurements.

References

Barnhart, T. B., Molotch, N. P., Livneh, B., Harpold, A. A., Knowles, J. F., and Schneider, D.: Snowmelt rate dictates streamflow, Geophysical Research Letters, 43, 8006–8016, https://doi.org/10.1002/2016GL069690, 2016.

Berghuijs, W., Woods, R., and Hrachowitz, M.: A precipitation shift from snow towards rain leads to a decrease in streamflow, Nature Climate Change, 4, 583–586, https://doi.org/10.1038/NCLIMATE2246, 2014.

Beria, H., Larsen, J. R., Ceperley, N. C., Michelon, A., Vennemann, T., and Schaefli, B.: Understanding snow hydrological processes through the lens of stable water isotopes, Wiley Interdisciplinary Reviews: Water, 5, e1311, https://doi.org/10.1002/wat2.1311, 2018.

Bernacchi, C., Singsaas, E., Pimentel, C., Portis Jr, A., and Long, S. P.: Improved temperature response functions for models of Rubisco-limited photosynthesis, Plant, Cell & Environment, 24, 253–259, https://doi.org/10.1111/j.1365-3040.2001.00668.x, 2001.

Blanken, P. and Black, T.: The canopy conductance of a boreal aspen forest, Prince Albert National Park, Canada, Hydrological Processes, 18, 1561–1578, https://doi.org/10.1002/hyp.1406, 2004.

Boisvenue, C. and Running, S. W.: Impacts of climate change on natural forest productivity–evidence since the middle of the 20th century, Global Change Biology, 12, 862–882, https://doi.org/10.1111/j.1365-2486.2006.01134.x, 2006.

Boivin, S. and Bégin, Y.: Development of a black spruce (Picea mariana) shoreline stand in relation to snow level variations at Lake Bienville in northern Quebec, Canadian Journal of Forest Research, 27, 295–303, 1997.

Boucher, É., Guiot, J., Hatté, C., Daux, V., Danis, P.-A., and Dussouillez, P.: An inverse modeling approach for tree-ring-based climate reconstructions under changing atmospheric CO_2 concentrations, Biogeosciences, 11, 3245–3258, https://doi.org/10.5194/bg-11-3245-2014, 2014.

Boucher, E., Nicault, A., Arseneault, D., Bégin, Y., and Karami, M.: Decadal variations in Eastern Canada's taiga wood biomass production forced by ocean-atmosphere interactions, Scientific Reports, 7, https://doi.org/10.1038/s41598-017-02580-9, 2017.

Buhay, W., Edwards, T., and Aravena, R.: Evaluating kinetic fractionation factors used for ecologic and paleoclimatic reconstructions from oxygen and hydrogen isotope ratios in plant water and cellulose, Geochimica et Cosmochimica Acta, 60, 2209–2218, https://doi.org/10.1016/0016-7037(96)00073-7, 1996.

Cernusak, L. A. and English, N. B.: Beyond tree-ring widths: stable isotopes sharpen the focus on climate responses of temperate forest trees, Tree physiology, 35, 1–3, https://doi.org/10.1093/treephys/tpu115, 2015.

Coulthard, B. L., Anchukaitis, K. J., Pederson, G. T., Cook, E., Littell, J., and Smith, D. J.: Snowpack signals in North American tree rings, Environmental Research Letters, 16, 034 037, https://doi.org/10.1088/1748-9326/abd5de, 2021.

Craig, H. and Gordon, L. I.: Deuterium and oxygen 18 variations in the ocean and the marine atmosphere, 1965.

Danis, P.-A., Hatté, C., Misson, L., and Guiot, J.: MAIDENiso: a multiproxy biophysical model of tree-ring width and oxygen and carbon isotopes, Canadian journal of forest research, 42, 1697–1713, https://doi.org/10.1139/x2012-089, 2012.

De Pury, D. and Farquhar, G.: Simple scaling of photosynthesis from leaves to canopies without the errors of big-leaf models, Plant, Cell & Environment, 20, 537–557, https://doi.org/10.1111/j.1365-3040.1997.00094.x, 1997.

DeNiro, M. J. and Epstein, S.: Relationship between the oxygen isotope ratios of terrestrial plant cellulose, carbon dioxide, and water, Science, 204, 51–53, https://doi.org/10.1126/science.204.4388.51, 1979.

D'Orangeville, L., Houle, D., Duchesne, L., Phillips, R. P., Bergeron, Y., and Kneeshaw, D.: Beneficial effects of climate warming on boreal tree growth may be transitory, Nature communications, 9, 1–10, https://doi.org/10.1038/s41467-018-05705-4, 2018.

Drew, D. M., Downes, G. M., and Battaglia, M.: CAMBIUM, a process-based model of daily xylem development in Eucalyptus, Journal of Theoretical Biology, 264, 395–406, https://doi.org/10.1016/j.jtbi.2010.02.013, 2010.

Du, J., He, Z., Yang, J., Chen, L., and Zhu, X.: Detecting the effects of climate change on canopy phenology in coniferous forests in semi-arid mountain regions of China, International journal of remote sensing, 35, 6490–6507, https://doi.org/10.1080/01431161.2014.955146, 2014.

Farquhar, G., Hubick, K., Condon, A., and Richards, R.: Carbon isotope fractionation and plant water-use efficiency, in: Stable isotopes in ecological research, pp. 21–40, Springer, 1989.

Farquhar, G., Barbour, M., and Henry, B.: Interpretation of oxygen isotope composition of leaf material, in: Stable isotopes: Integration of Biological, Ecological and Geochemical Processes, pp. 27–62, Garland Science, 1998.

Farquhar, G. D., von Caemmerer, S. v., and Berry, J. A.: A biochemical model of photosynthetic CO_2 assimilation in leaves of C_3 species, Planta, 149, 78–90, https://doi.org/10.1007/bf00386231, 1980.

Field, R., Andreu-Hayles, L., D'Arrigo, R., Oelkers, R., Luckman, B., Morimoto, D., Boucher, E., Gennaretti, F., Hermoso, I., Lavergne, A., et al.: Tree-ring Cellulose δ18O Records Similar Large-scale Climate Influences as Precipitation δ18O in the Northwest Territories of Canada, Climate Dynamics, https://doi.org/10.21203/rs.3.rs-214162/v1, 2021.

Fritts, H. C., Vaganov, E. A., Sviderskaya, I. V., and Shashkin, A. V.: Climatic variation and tree-ring structure in conifers: empirical and mechanistic models of tree-ring width, number of cells, cell size, cell-wall thickness and wood density, Climate Research, pp. 97–116, https://doi.org/10.3354/cr001097, 1991.

Gaucherel, C., Campillo, F., Misson, L., Guiot, J., and Boreux, J.-J.: Parameterization of a process-based tree-growth model: comparison of optimization, MCMC and particle filtering algorithms, Environmental Modelling & Software, 23, 1280–1288, https://doi.org/10.1016/j.envsoft.2008.03.003, 2008.

Gea-Izquierdo, G., Guibal, F., Joffre, R., Ourcival, J., Simioni, G., and Guiot, J.: Modelling the climatic drivers determining photosynthesis and carbon allocation in evergreen Mediterranean forests using multiproxy long time series, https://doi.org/10.5194/bg-12-3695-2015, 2015.

Gennaretti, F., Gea-Izquierdo, G., Boucher, E., Berninger, F., Arseneault, D., and Guiot, J.: Ecophysiological modeling of the climate imprint on photosynthesis and carbon allocation to the tree stem in the North American boreal forest, Biogeosciences Discuss, pp. 1–26, https://doi.org/10.5194/bg-2017-51, 2017a.

Gennaretti, F., Huard, D., Naulier, M., Savard, M., Bégin, C., Arseneault, D., and Guiot, J.: Bayesian multiproxy temperature reconstruction with black spruce ring widths and stable isotopes from the northern Quebec taiga, Climate Dynamics, 0, 1–13, https://doi.org/10.1007/s00382-017-3565-5, 2017b.

Girardin, M. P., Raulier, F., Bernier, P. Y., and Tardif, J. C.: Response of tree growth to a changing climate in boreal central Canada: a comparison of empirical, process-based, and hybrid modelling approaches, Ecological modelling, 213, 209–228, https://doi.org/10.1029/2010JG001287, 2008.

Guiot, J., Boucher, E., and Gea-Izquierdo, G.: Process models and model-data fusion in dendroecology, Frontiers in Ecology and Evolution, 2, 52, https://doi.org/10.3389/fevo.2014.00052, 2014.

Helliker, B. R. and Richter, S. L.: Subtropical to boreal convergence of tree-leaf temperatures, Nature, 454, 511–514, https://doi.org/10.1038/nature07031, 2008.

Hölttä, T., Mäkinen, H., Nöjd, P., Mäkelä, A., and Nikinmaa, E.: A physiological model of softwood cambial growth, Tree Physiology, 30, 1235–1252, https://doi.org/10.1093/treephys/tpq068, 2010.

Horita, J. and Wesolowski, D. J.: Liquid-vapor fractionation of oxygen and hydrogen isotopes of water from the freezing to the critical
temperature, Geochimica et Cosmochimica Acta, 58, 3425–3437, https://doi.org/10.1016/0016-7037(94)90096-5, 1994.

Hutchinson, M. F., McKenney, D. W., Lawrence, K., Pedlar, J. H., Hopkinson, R. F., Milewska, E., and Papadopol, P.: Development and
testing of Canada-wide interpolated spatial models of daily minimum–maximum temperature and precipitation for 1961–2003, Journal of
Applied Meteorology and Climatology, 48, 725–741, https://doi.org/10.1175/2008JAMC1979.1, 2009.

Jarvis, P. and Linder, S.: Constraints to growth of boreal forests, Nature, 405, 904–905, 2000.

Keeling, C. D., Bacastow, R. B., Bainbridge, A. E., Ekdahl Jr, C. A., Guenther, P. R., Waterman, L. S., and Chin, J. F.: Atmospheric carbon
dioxide variations at Mauna Loa observatory, Hawaii, Tellus, 28, 538–551, https://doi.org/10.3402/tellusa.v28i6.11322, 1976.

Knauer, J., Werner, C., and Zaehle, S.: Evaluating stomatal models and their atmospheric drought response in a land surface scheme: A
multibiome analysis, Journal of Geophysical Research: Biogeosciences, 120, 1894–1911, https://doi.org/10.1002/2015jg003114, 2015.

Kurita, N., Yoshida, N., Inoue, G., and Chayanova, E. A.: Modern isotope climatology of Russia: A first assessment, Journal of Geophysical
Research: Atmospheres, 109, https://doi.org/10.1029/2003jd003404, 2004.

Lavergne, A., Gennaretti, F., Risi, C., Daux, V., Boucher, E., Savard, M., Naulier, M., Villalba, R., Begin, C., and Guiot, J.: Modelling
tree ring cellulose δ^{18}O variations in two temperature-sensitive tree species from North and South America, Climate of the Past, 13,
1515–1526, https://doi.org/10.5194/cp-13-1515-2017, 2017.

Lawrence, D. M., Fisher, R. A., Koven, C. D., Oleson, K. W., Swenson, S. C., Bonan, G., Collier, N., Ghimire, B., van Kampenhout, L.,
Kennedy, D., et al.: The Community Land Model version 5: Description of new features, benchmarking, and impact of forcing uncertainty,
Journal of Advances in Modeling Earth Systems, 11, 4245–4287, https://doi.org/10.1029/2018MS001583, 2019.

Leuning, R., Kelliher, F. M., De Pury, D., and Schulze, E.-D.: Leaf nitrogen, photosynthesis, conductance and transpiration: scaling from
leaves to canopies, Plant, Cell & Environment, 18, 1183–1200, https://doi.org/10.1111/j.1365-3040.1995.tb00628.x, 1995.

Li, D., Wrzesien, M. L., Durand, M., Adam, J., and Lettenmaier, D. P.: How much runoff originates as snow in the western United States,
and how will that change in the future?, Geophysical Research Letters, 44, 6163–6172, https://doi.org/10.1002/2017GL073551, 2017.

Li, G., Harrison, S., Prentice, I., and Falster, D.: Simulation of tree-ring widths with a model for primary production, carbon allocation,
and growth, Biogeosciences, 11, 6711–6724, https://doi.org/10.5194/bg-11-6711-2014, https://bg.copernicus.org/articles/11/6711/2014/,
2014.

Loescher, H., Hanson, C., and Ocheltree, T.: The psychrometric constant is not constant: A novel approach to enhance the accuracy
and precision of latent energy fluxes through automated water vapor calibrations, Journal of Hydrometeorology, 10, 1271–1284,
https://doi.org/10.1175/2009JHM1148.1, 2009.

McCabe, G. J. and Wolock, D. M.: Recent declines in western US snowpack in the context of twentieth-century climate variability, Earth
Interactions, 13, 1–15, https://doi.org/10.1175/2009EI283.1, 2009.

Meredith, M., Sommerkorn, M., Cassotta, S., Derksen, C., Ekaykin, A., Hollowed, A., Kofinas, G., Mackintosh, A., Melbourne-Thomas, J.,
Muelbert, M., et al.: Polar Regions. Chapter 3, IPCC Special Report on the Ocean and Cryosphere in a Changing Climate, 2019.

Mesinger, F., DiMego, G., Kalnay, E., Mitchell, K., Shafran, P. C., Ebisuzaki, W., Jović, D., Woollen, J., Rogers, E., Berbery, E. H., et al.:
North American regional reanalysis, Bulletin of the American Meteorological Society, 87, 343–360, https://doi.org/10.1175/BAMS-87-3-
343, 2006.

Miller, J. R., Russell, G. L., and Caliri, G.: Continental-scale river flow in climate models, Journal of Climate, 7, 914–928,
https://doi.org/10.1175/1520-0442(1994)007<0914:CSRFIC>2.0.CO;2, 1994.

Misson, L.: MAIDEN: a model for analyzing ecosystem processes in dendroecology, Canadian Journal of Forest Research, 34, 874–887, https://doi.org/10.1139/x03-252, 2004.

Nash, J. E. and Sutcliffe, J. V.: River flow forecasting through conceptual models part I—A discussion of principles, Journal of hydrology, 10, 282–290, 1970.

600   Naulier, M., Savard, M. M., Bégin, C., Marion, J., Arseneault, D., and Bégin, Y.: Carbon and oxygen isotopes of lakeshore black spruce trees in northeastern Canada as proxies for climatic reconstruction, Chemical Geology, 374, 37–43, 2014.

Naulier, M., Savard, M. M., Bégin, C., Gennaretti, F., Arseneault, D., Marion, J., Nicault, A., and Bégin, Y.: A millennial summer temperature reconstruction for northeastern Canada using oxygen isotopes in subfossil trees, Climate of the Past, 11, 1153–1164, https://doi.org/10.5194/cp-11-1153-2015, 2015a.

605   Naulier, M., Savard, M. M., Bégin, C., Marion, J., Nicault, A., and Bégin, Y.: Temporal instability of isotopes–climate statistical relationships–A study of black spruce trees in northeastern Canada, Dendrochronologia, 34, 33–42, 2015b.

Nicault, A., Boucher, E., Bégin, C., Guiot, J., Marion, J., Perreault, L., Roy, R., Savard, M. M., and Bégin, Y.: Hydrological reconstruction from tree-ring multi-proxies over the last two centuries at the Caniapiscau Reservoir, northern Québec, Canada, Journal of Hydrology, 513, 435–445, https://doi.org/10.1016/j.jhydrol.2014.03.054, 2014.

610   Nicault, A., Boucher, E., Tapsoba, D., Arseneault, D., Berninger, F., Bégin, C., DesGranges, J.-L., Guiot, J., Marion, J., Wicha, S., et al.: Spatial analysis of black spruce (Picea mariana (Mill.) BSP) radial growth response to climate in northern Québec–Labrador Peninsula, Canada, Canadian Journal of Forest Research, 45, 343–352, 2015.

Nossent, J. and Bauwens, W.: Application of a normalized Nash-Sutcliffe efficiency to improve the accuracy of the Sobol'sensitivity analysis of a hydrological model, Mathematics and Computers in Simulation, 55, 271–280, 2011.

615   Oki, T., Nishimura, T., and Dirmeyer, P.: Assessment of annual runoff from land surface models using Total Runoff Integrating Pathways (TRIP), Journal of the Meteorological Society of Japan. Ser. II, 77, 235–255, https://doi.org/10.2151/jmsj1965.77.1B_235, 1999.

Ols, C., Trouet, V., Girardin, M. P., Hofgaard, A., Bergeron, Y., and Drobyshev, I.: Post-1980 shifts in the sensitivity of boreal tree growth to North Atlantic Ocean dynamics and seasonal climate, Global and planetary change, 165, 1–12, 2018.

Perkins, D. L. and Swetnam, T. W.: A dendroecological assessment of whitebark pine in the Sawtooth–Salmon River region, Idaho, Canadian

620   Journal of Forest Research, 26, 2123–2133, https://doi.org/10.1139/x26-241, 1996.

Peters, W., Jacobson, A. R., Sweeney, C., Andrews, A. E., Conway, T. J., Masarie, K., Miller, J. B., Bruhwiler, L. M., Pétron, G., Hirsch, A. I., et al.: An atmospheric perspective on North American carbon dioxide exchange: CarbonTracker, Proceedings of the National Academy of Sciences, 104, 18 925–18 930, https://doi.org/10.1073/pnas.0708986104, 2007.

Peterson, D. W. and Peterson, D. L.: Effects of climate on radial growth of subalpine conifers in the North Cascade Mountains, Canadian

625   Journal of Forest Research, 24, 1921–1932, https://doi.org/10.1139/x94-247, 1994.

Porter, T. J., Pisaric, M. F., Field, R. D., Kokelj, S. V., Edwards, T. W., deMontigny, P., Healy, R., and LeGrande, A. N.: Spring-summer temperatures since AD 1780 reconstructed from stable oxygen isotope ratios in white spruce tree-rings from the Mackenzie Delta, northwestern Canada, Climate Dynamics, 42, 771–785, https://doi.org/10.1007/s00382-013-1674-3, 2014.

Rathgeber, C., Nicault, A., Kaplan, J. O., and Guiot, J.: Using a biogeochemistry model in simulating forests productivity responses to

630   climatic change and [CO2] increase: example of Pinus halepensis in Provence (south-east France), Ecological modelling, 166, 239–255, https://doi.org/10.1016/S0304-3800(03)00161-3, 2003.

Roden, J. S. and Ehleringer, J. R.: Hydrogen and oxygen isotope ratios of tree ring cellulose for field-grown riparian trees, Oecologia, 123, 481–489, https://doi.org/10.1007/s004420000349, 2000.

Running, S. W., Nemani, R. R., and Hungerford, R. D.: Extrapolation of synoptic meteorological data in mountainous terrain and its use for simulating forest evapotranspiration and photosynthesis, Canadian Journal of Forest Research, 17, 472–483, https://doi.org/10.1139/x87-081, 1987.

Rutter, N., Essery, R., Pomeroy, J., Altimir, N., Andreadis, K., Baker, I., Barr, A., Bartlett, P., Boone, A., Deng, H., et al.: Evaluation of forest snow processes models (SnowMIP2), Journal of Geophysical Research: Atmospheres, 114, 2009.

Saurer, M., Aellen, K., and Siegwolf, R.: Correlating δ13C and δ18O in cellulose of trees, Plant, Cell & Environment, 20, 1543–1550, https://doi.org/10.1046/j.1365-3040.1997.d01-53.x, 1997.

Southworth, F., Peterson, B., and Lambert, B.: Development of a regional routing model for strategic waterway analysis, Transportation research record, 1993, 109–116, https://doi.org/10.3141/1993-15, 2007.

St. George, S., Meko, D. M., Girardin, M.-P., MacDonald, G. M., Nielsen, E., Pederson, G. T., Sauchyn, D. J., Tardif, J. C., and Watson, E.: The tree-ring record of drought on the Canadian Prairies, Journal of Climate, 22, 689–710, https://doi.org/10.1175/2008JCLI2441.1, 2009.

Sternberg, L. D. S., Deniro, M. J., and Savidge, R. A.: Oxygen isotope exchange between metabolites and water during biochemical reactions leading to cellulose synthesis, Plant Physiology, 82, 423–427, https://doi.org/10.1104/pp.82.2.423, 1986.

Stigter, E. E., Litt, M., Steiner, J. F., Bonekamp, P. N., Shea, J. M., Bierkens, M. F., and Immerzeel, W. W.: The importance of snow sublimation on a Himalayan glacier, Frontiers in Earth Science, Cryosphere, 6, https://doi.org/10.3389/feart.2018.00108, 2018.

Szejner, P., Wright, W. E., Belmecheri, S., Meko, D., Leavitt, S. W., Ehleringer, J. R., and Monson, R. K.: Disentangling seasonal and interannual legacies from inferred patterns of forest water and carbon cycling using tree-ring stable isotopes, Global change biology, 24, 5332–5347, https://doi.org/10.1111/gcb.14395, 2018.

Ueyama, M., Iwata, H., and Harazono, Y.: AmeriFlux US-Uaf University of Alaska, Fairbanks, Ver. 8.5, https://doi.org/10.17190/AMF/1480322, https://ameriflux.lbl.gov/doi/AmeriFlux/US-Uaf, 2021.

van Kampenhout, L., Lenaerts, J. T., Lipscomb, W. H., Sacks, W. J., Lawrence, D. M., Slater, A. G., and van den Broeke, M. R.: Improving the representation of polar snow and firn in the Community Earth System Model, Journal of Advances in Modeling Earth Systems, 9, 2583–2600, https://doi.org/10.1002/2017MS000988, 2017.

Woodhouse, C. A.: A 431-yr reconstruction of western Colorado snowpack from tree rings, Journal of Climate, 16, 1551–1561, https://doi.org/10.1175/1520-0442(2003)016<1551:AYROWC>2.0.CO;2, 2003.

Yakir, D.: Variations in the natural abundance of oxygen-18 and deuterium in plant carbohydrates, Plant, Cell & Environment, 15, 1005–1020, https://doi.org/10.1111/j.1365-3040.1992.tb01652.x, 1992.

Yoshimura, K., Kanamitsu, M., Noone, D., and Oki, T.: Historical isotope simulation using reanalysis atmospheric data, Journal of Geophysical Research: Atmospheres, 113, https://doi.org/10.1029/2008JD010074, 2008.

Site	Precipitation type	a (‰ °C^{-1})	b (‰ mm^{-1})	c (‰)
Tungsten	Snowfall	0.4124	-0.0631	-16.4182
	Rainfall	0.4583	-0.9909	-16.26
Caniapiscau	Snowfall	0.4007	-1.622	-13.1279
	Rainfall	0.2654	-0.3613	-11.4665

Table 1. Parameters obtained for the regression models for snow and rainfall using the IsoGSM dataset at the Tungsten and Caniapiscau sites.

Parameter	Units	Prior range	Posterior - Tungsten Without snow	Posterior - Tungsten With snow	Posterior - Caniapiscau Without snow	Posterior - Caniapiscau With snow
r_a	s m^{-1}	0/400		85.91/90.50 (87.35)		44.94/50.83 (47.88)
f_0	n/a	0.3/0.5	0.30/0.42 (0.32)	0.37/0.5 (0.48)	0.30/0.43 (0.32)	0.33/0.49 (0.43)
ϵ_0	‰	24/30	25.43/28.42 (27.85)	25.36/27.67 (27.41)	24.03/26.36 (24.48)	24.02/25.51 (24.15)
ϵ_k	‰	10/30	10.91/25.15 (13.03)	10.37/22.83 (11.81)	14.07/26.52 (22.77)	16.23/26.48 (23.41)

Table 2. Calibration parameters for the snowpile (for the version with snow exclusively) and $\delta^{18}O_{TRC}$. Parameters, units, prior range, and posterior range (with parameter value in the plausible block) for both MAIDENiso versions and both sites.
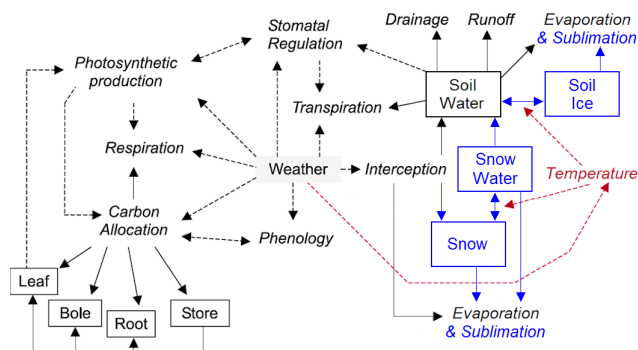
Figure 1. Diagram showing the main features in the new version of MAIDENiso, with old components and fluxes in black and new ones in blue for snow/ice and in red for the thermal module. Processes are in italics, boxes are carbon and water pools, broken lines are links between processes, and solid lines are carbon and water fluxes. Figure modified from Misson (2004).
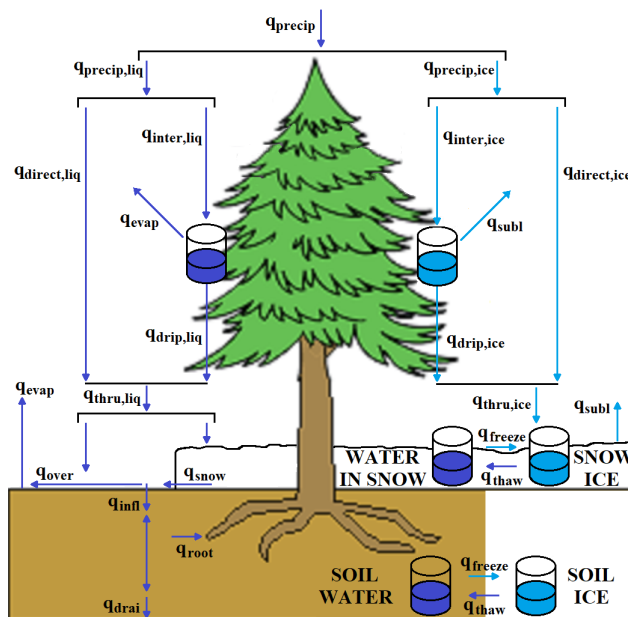
Figure 2. The hydrological system in the new version of MAIDENiso. Pools (flasks) and fluxes (arrows) are shown for liquid water in dark blue, and for snow/ice in light blue.
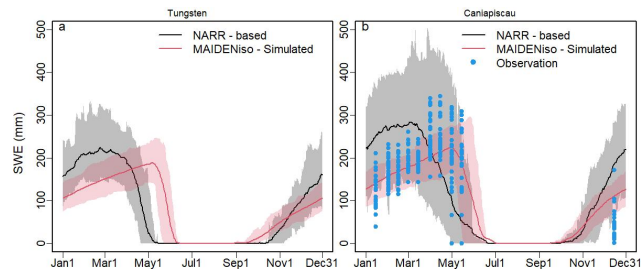
Figure 3. Snow Water Equivalent (SWE) averaged over 1979-1997 at the (a) Tungsten and (b) Caniapiscau sites, calculated from the NARR data (black) and simulated by MAIDENiso (red) using NARR meteorology. The solid line indicates the average of the same DOY during this period, and the shadows indicate the 2σ variability. Direct observations of SWE at Caniapiscau, taken at discrete intervals, are shown as blue dots.
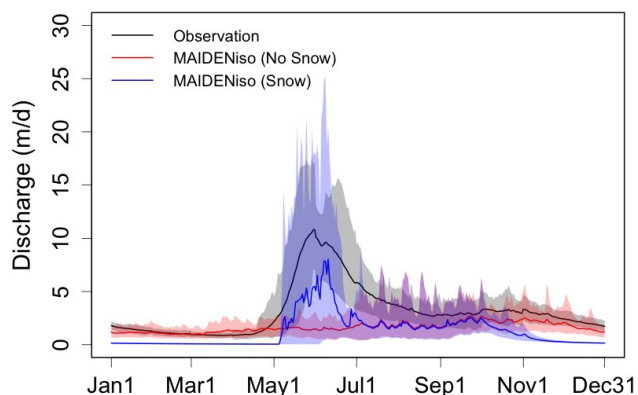
Figure 4. Water outflux (drainage + runoff) simulated for 1979-1997 in the Caniapiscau site by MAIDENiso (smoothed over a 10-day period), without (red) and with (blue) the snow module. The black line shows the discharge from observations from the Caniapiscau basin between 1979-1997, scaled with the area of the basin. Solid lines indicate the average of the same DOY during this period, shadows indicate the 2σ variability.
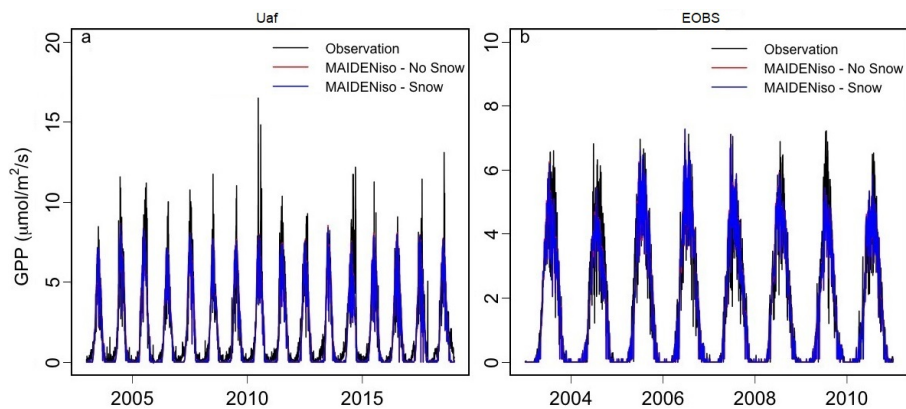
Figure 5. GPP at the Uaf site (a) and the EOBS site (b). We show observations from flux towers (black) and MAIDENiso simulations without (red) and with (blue) snow processes. Independent optimizations are run for the two versions of MAIDENiso.
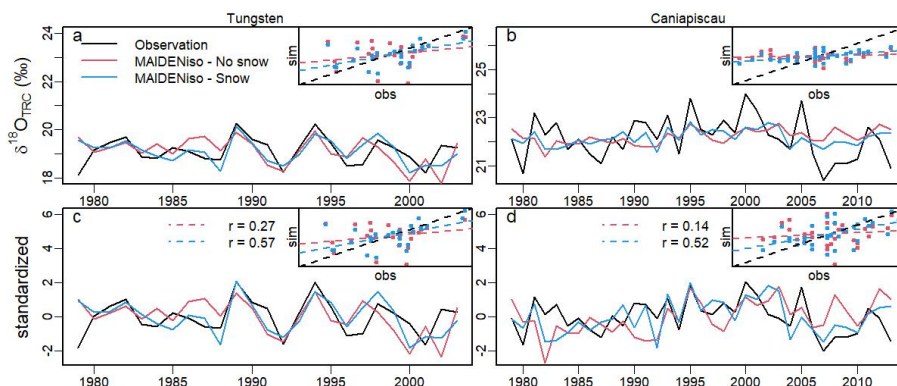
Figure 6. $\delta^{18}O_{TRC}$ observed (black) and simulated by the versions of MAIDENiso without (red) and with (blue) snow, using the calibrated parameters for (a,c) Tungsten and (b,d) Caniapiscau. Top panels show the raw $\delta^{18}O_{TRC}$ series, bottom panels show the standardized $\delta^{18}O_{TRC}$ series. Top-right inner panels show the scatter diagrams of the simulated (by both versions of the model, red for the version without snow and blue for the version with snow) and observed values of $\delta^{18}O_{TRC}$, with dashed lines showing the linear regression models. Correlations are identical for the raw series (top panels) and the standardized series (bottom panels).
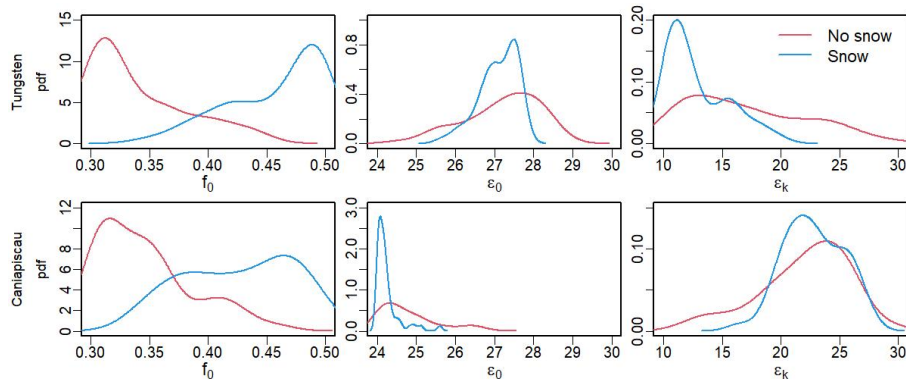
Figure 7. Posterior probability density distributions of the parameters controlling $\delta^{18}O_{\mathrm{TRC}}$ at the Tungsten and Caniapiscau sites, for the model without (red) and with (blue) snow.
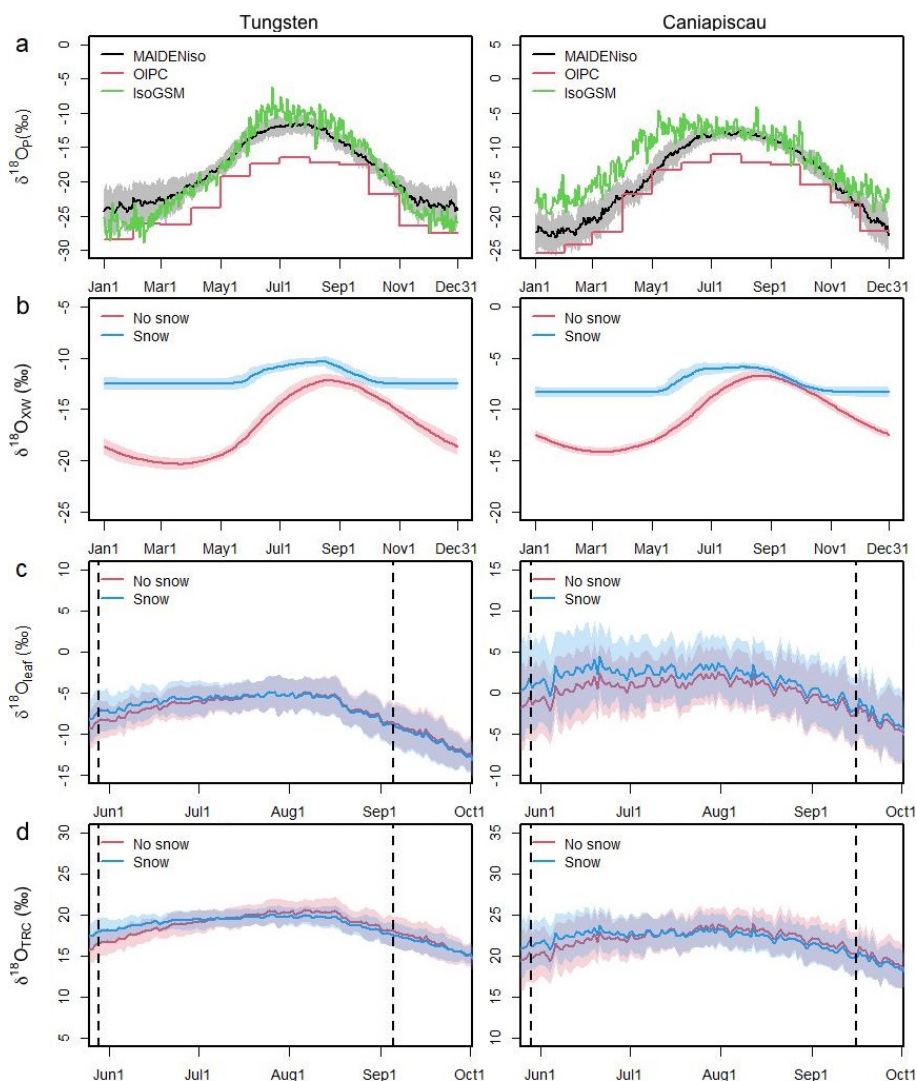
Figure 8. Simulated of $\delta^{18}O$ at different stages of the water cycle for the period 1979-2003, for the sites of Tungsten (left) and Caniapiscau (right). a) The $\delta^{18}O$ in precipitation ($\delta^{18}O_P$) simulated by MAIDENiso using the NARR meteorology (black), monthly data from the Online Isotopes in Precipitation Calculator (OIPC, red) and mean from the IsoGSM dataset (green). b) The $\delta^{18}O$ in the xylem water ($\delta^{18}O_{XW}$), c) The $\delta^{18}O$ in the leaf ($\delta^{18}O_{leaf}$) and d) in the Tree-Ring Cellulose ($\delta^{18}O_{TRC}$), for the model without snow (red) and with snow (blue). Shadows indicate the 2σ variability for the same DOY within the 1979-2003 period. Vertical dashed lines in c) and d) indicate the start (budburst) and end of the growth season. Note that isotopic calculations are still made outside of this period but no water is absorbed by the tree.
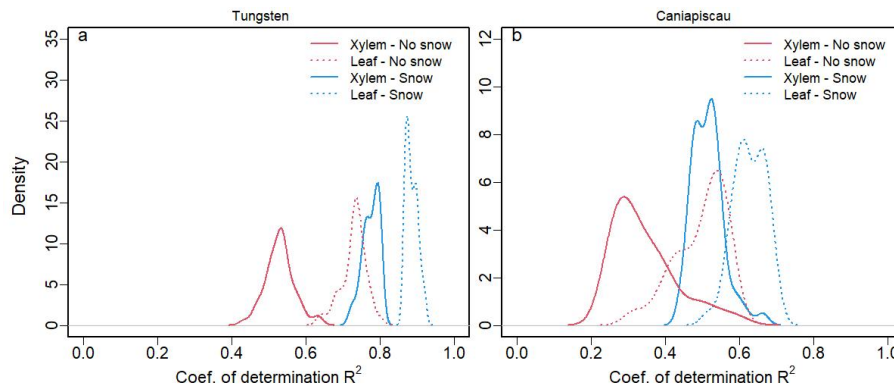
Figure 9. Density distribution of the coefficients of determination (R^2) between the reference simulations and the water source (xylem) experiments (solid line, $\delta^{18}O_V$ and h_{air} set constant), and the leaf water enrichment experiments (dashed line, $\delta^{18}O_{XW}$ set constant), for the model without snow (red) and with snow (blue). Shown for a) Tungsten and b) Caniapiscau.

Parameter	Units	Prior range	Posterior - EOBS Without snow	Posterior - EOBS With snow	Posterior - Uaf Without snow	Posterior - Uaf With snow
Vmax	μmolC m^{-2} s^{-1}	5/150	47/128 (59)	47/125 (66)	82/149 (141)	82/147 (101)
Vb	n/a	-0.30/-0.10	-0.22/-0.15 (-0.18)	-0.22/-0.15 (-0.17)	-0.25/-0.20 (-0.21)	-0.26/-0.20 (-0.22)
Vip	°C	10/30	15.5/26.3 (18.2)	15.8/26.1 (19.4)	18.9/23.6 (22.8)	18.7/23.4 (20.5)
soilb	n/a	0.025/-0.005	-0.023/-0.005 (-0.02)	-0.023/-0.006 (-0.013)	-0.023/-0.006 (-0.021)	-0.021/-0.006 (-0.021)
soilip	mm	100/400	111/312 (179)	120/260 (177)	109/251 (161)	102/273 (179)
τ	days	1/20	12.7/17.1 (15.1)	12.6/16.7 (15.1)	13.8/17.1 (16.5)	13.5/17.5 (15.0)

Table A1. Calibration parameters for the GPP module. Parameters, units, prior range, and posterior range (with parameter value in the plausible block) for both MAIDENiso versions and both flux towers.
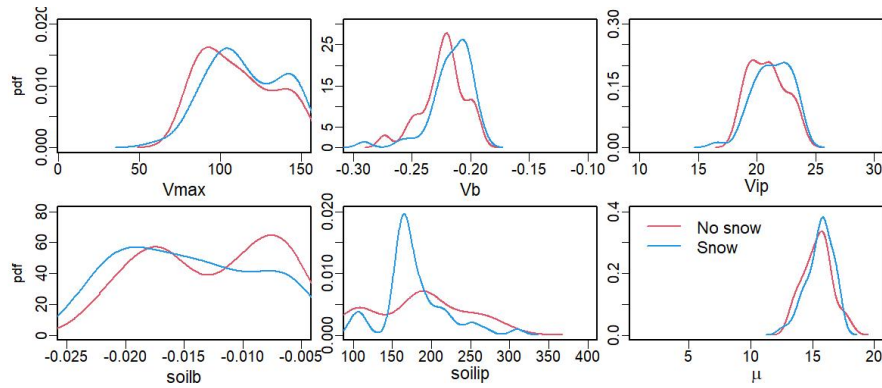
Figure A1. Posterior probability density distributions of the parameters controlling GPP at the Uaf site, for the model without (red) and with (blue) snow.
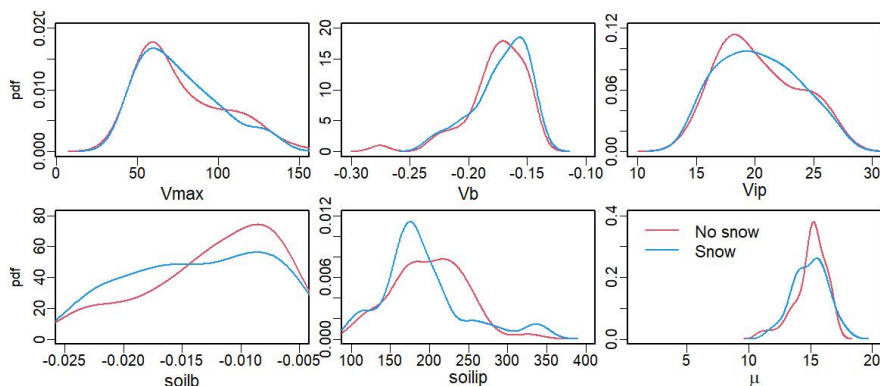
Figure A2. Posterior probability density distributions of the parameters controlling GPP at the EOBS site, for the model without (red) and with (blue) snow.